Temporal and Spatial Trends in the MODIS-derived Spatially Complete Global Spectral Surface Albedo Products

ERIC G. MOODY,* MICHAEL D. KING,+ CRYSTAL B. SCHAAF,#
AND STEVEN PLATNICK+

*RS Information Systems, Inc., Lanham, Maryland
+Earth Sciences Division, NASA Goddard Space Flight Center, Greenbelt, Maryland
#Center for Remote Sensing, Department of Geography, Boston University, Boston, Massachusetts

Journal of Climate

(Manuscript submitted October 2006)

Corresponding author address: Eric G. Moody, RS Information Systems, Inc., Lanham, MD 20706 USA.

E-mail: moody@climate.gsfc.nasa.gov.

ABSTRACT

Five years of spatially complete ephemeral and seasonal snow-free land surface albedo data have been prepared using high quality diffuse bihemispherical (white-sky) and direct-beam directional hemispherical (black-sky) land surface albedo data (MOD43B3) derived from observations taken by the MODIS instrument aboard NASA's Terra satellite platform. In addition, a five-year aggregate climatology product was generated. These spatially complete products were prepared using an ecosystem-dependant temporal interpolation technique that has been shown previously to replace missing data within 3-8% error.

In brief, the technique is predicated upon the concept that within a local region, pixels of the same ecosystem classification should exhibit roughly the same phenological, or temporal, behavior. Variations in climate and soil conditions, however, result in pixel-to-pixel differences in the relative magnitudes of the behavioral curves. In order to maintain these variations in magnitude, missing data are filled by imposing only the shape of the pixel's ecosystem phenological curve onto any temporal data that exists for that pixel; these local-to-regional phenological curves are based on the MODIS IGBP land cover classification product geolocated with high-quality MOD43B3 data.

In the ensuing analysis, filled and MOD43B3 albedo products are examined through comparing temporal and spatial trends. The analysis illustrates the percentage of data (spatially, temporally, and by ecosystem classification) that is filled. Further, the analysis demonstrates that the MOD43B3 and filled data exhibit qualitatively similar large scale phenological behavior. Closer inspection reveals that discrepancies in trends arise when small MOD43B3 or filled pixel sample sizes are disproportionately distributed across a latitude belt. Such cases allow a few dominant regions to skew latitude belt mean calculations; these cases

thereby serve to showcase the inherent spectral, spatial, and temporal variability in the MOD43B3 data as well as the ability of the fill technique to maintain these unique regional and pixel-level phenological characteristics.

1. Introduction

Among inputs into various earth system modeling and remote sensing efforts, spatially complete ephemeral and seasonal snow-free land surface albedo data are critical as they describe the radiative properties of the earth's surface. Albedo represents the ratio of reflected to incoming solar radiation at the earth's surface. It has proven to be important for a variety of projects including the remote sensing of cloud properties (King et al. 1992, 2003, 2004; Platnick et al. 2003) and aerosol properties (Kaufman et al. 1997; King et al. 1999; Hsu et al. 2004) from satellite and airborne platforms, as well as analysis of aerosol optical properties from surface-based sun/sky radiometers (Holben et al. 1998; Dubovik et al. 2000). Spectral surface reflectance properties are also useful in biophysically-based land surface modeling of the exchange of energy, water, momentum, and carbon for various land use categories (Sellers et al. 1996; Bounoua et al. 2002), and in studies of surface energy balance (Ingram et al. 1989; Dirmeyer et al. 1994; Whitlock et al. 1995). The modeling community requires values of snow-free surface albedo to initialize their models and therefore needs remotely sensed data that have had all ephemeral and seasonal snow effects removed.

Diffuse bihemispherical (white-sky) and direct-beam directional hemispherical (black-sky) land surface albedo data, known as MOD43B3 (Schaaf et al. 1998), have been derived from observations taken by the Moderate Resolution Imaging Spectroradiometer (MODIS) onboard NASA's Terra (King and Herring 2000) spacecraft. Beginning on February 24, 2000, this data product has provided global values every 16 days at 1 km spatial resolution for the first seven MODIS bands, 0.47 through 2.1 μm, and for three broadband wavelengths, 0.3-0.7, 0.3-5.0, and 0.7-5.0 μm. The products have been validated (Liang et al. 2002; Jin et al. 2003a, 2003b; Wang et al. 2004), and the collection 4 reprocessed data are distin-

guished as "Validated – Stage 1."

As described in Moody et al. (2005), roughly 30% of the global land surface on an annual equal-angle basis is obscured due to persistent and transient cloud cover, while another 20% is obscured due to ephemeral and seasonal snow effects. To provide researchers with a spatially complete global snow-free land surface albedo dataset that they require, an ecosystem-dependant temporal interpolation technique was developed to fill missing or lower quality data and snow covered values from the official MOD43B3 dataset with geophysically realistic values.

The technique is based upon the concept that within a limited region, pixels of the same ecosystem classification should exhibit roughly the same phenological, or temporal, behavior (Reed et al. 1994; Kaduk and Heimann 1996; Schwartz 1998; Schwartz and Reed 1999; White et al. 1997; Zhang et al. 2003; Penuelas et al. 2004). Variations in climate and soil conditions, however, result in pixel-to-pixel differences in the relative magnitudes of the behavioral curves. In order to maintain these spatial pixel-level variations in a temporal sense, missing data are filled in by imposing the shape of the pixel's ecosystem classification phenological curve onto any temporal data that do exist for that pixel. Moody et al. (2005) showed that this technique replaces missing data with values that have only 3-8% error.

The purpose of this paper is to refine and apply the ecosystem-dependent temporal interpolation technique to five years of collection 4 MOD43B3 albedo data, years 2000-2004. This will provide researchers with ephemeral and seasonal snow-free spatially complete land surface albedo data with the interannual variability required for detailed studies. In addition, the technique is applied to a five-year aggregate of MOD43B3 data to provide researchers with a climatol-

ogy, or average year.

This paper builds upon the error analysis presented in Moody et al. (2005) by qualitatively comparing temporal and spatial trends of pixels that have been filled versus pixels flagged as original high-quality MOD43B3 data. The analysis showcases the ability of the filling technique to maintain regional and pixel-level spatial, spectral, and temporal behavior that is inherent in the MOD43B3 data. These comparisons will be made for a single-year of filled data, year 2002, and for the five-year aggregate climatology product.

2. Spatially complete products

The algorithm to fill MOD43B3 data has been refined to better prescribe areas with few observations, namely cloud covered tropical regions and high latitude areas impacted by ephemeral and seasonal snow. An updated MODIS International Geosphere-Biosphere Programme (IGBP) ecosystem classification dataset (Friedl et al. 2002), referred to as product MOD12Q1 (annual Collection 4, year 2001, day 001) is used that, among other improvements, has dramatically improved the classification of urban areas.

The following subsections will describe the refinement of the fill methodology, as applied to the five-year aggregate climatology, and the inclusion of statistics from the aggregate climatology to assist in processing areas of few observations in the five individual years.

a. Refinements in the fill methodology

As described in Moody et al. (2005), the MOD43B3 data are projected onto a 1° equal angle grid and further conditioned to remove pixels of lesser quality and pixels flagged as ephemeral and seasonal snow. Statistics are computed from the resulting ephemeral and seasonal snow-free and high quality albedo data. These

statistics are subsequently used to generate ecosystem dependent local and regional phenological behavior. The interpolation technique is then applied to each pixel by imposing the shape only, not the magnitude, of the appropriate phenological behavior onto any existing pixel-level data. The pixel's missing temporal data are then filled with the selected local-to-regional phenological behavior that best represents the pixel's temporal information.

While the application of the technique is effective in general, proper prescription of the dormant state of high latitude Northern Hemisphere winter pixels remains elusive. In these areas, the beginning of the growth/end of the senescence states and the dormant state is often obscured due to cloud cover and ephemeral and seasonal snow onset, even for local and regional statistics. Fortunately, however, pixels in these areas typically have a single growth cycle and the full maturation state is usually observed. As such, a pixel's dormant state can be approximated, as described in Moody et al. (2005), as a percentage of the summer extrema; in brief, wavelength- and ecosystem-dependant percentages are computed a priori as averages of high latitude pixels that exhibit full maturation and dormant states. To complete the process, the pixel's first/last 16-day period of the year is set to the approximated value and then the temporal behavior is prescribed.

Unfortunately, ephemeral and seasonal snow contaminated albedo values and the least-squares polynomial fit calculation can result in unphysical dormant states. To resolve this issue, the phenological behavior is screened to ensure physical behavior. For each fitted phenological curve, the dormant and early growth/late senescent mean values are computed from three dormant 16-day periods (either periods 65-97 or 289-321) and three near mature/early senescent 16-day periods (either periods 129-161 or 225-257). A percentage change is com-

puted and compared to the percentage of the summer extreme value. If the trends are opposite, then the curve is removed from consideration as it is deemed to be decaying in an unphysical manner.

Additional refinements include using the five-year aggregate MOD43B3 data in areas of limited temporal coverage (i.e. high latitude ephemeral and seasonal snow-covered areas and tropical regimes). The added temporal coverage of these statistics provides a more robust description of the temporal behavior.

b. Five-year aggregate climatology product

The spatially complete five-year (2000-2004) aggregate climatology product is generated by first aggregating the highest quality ephemeral and seasonal snow-free MOD43B3 retrievals. For each pixel in each 16-day period, an average is computed for valid data from each of the five years. The resulting ephemeral and seasonal snow-free aggregate dataset is comprised of diffuse bihemispherical (white-sky) and direct-beam directional hemispherical (black-sky) albedo for 23 16-day periods, from days 001 to 353, for each of the original 10 bands in the MOD43B3 product.

Ecosystem-dependent local and regional statistics of the winter percentage of the summer extreme values for each ecosystem class are computed from the aggregate MOD43B3 data. The refined temporal interpolation technique (Moody et al. (2005), and discussed in Section 2.a) is then applied to these data to generate the spatially complete five-year aggregate climatology.

c. Single-year product

Five single-year MOD43B3 data (2000, 2001, …, 2004) are likewise processed with the refined temporal interpolation technique to provide 5 consecutive years of spatially complete albedo data. In addition to the refinements described

above, the five-year aggregate MOD43B3 data have been incorporated into the single-year processing to assist in areas with limited temporal coverage. These areas include high latitude ephemeral and seasonal snow impacted regions and tropical persistent cloud regions.

As will be described in Section 3 (Fig. 1), the five-year aggregate MOD43B3 data have better temporal coverage that results in more robust temporal trends. As such, the aggregate MOD43B3 data can be used in three ways. First, in high latitudes, the percentage of the summer extrema albedo computed from a single year is replaced with the five-year aggregate value. Also in northern high latitudes (>40°), each pixel's data during dormant periods (16-day periods beginning on days 001-129 and 241-353) with missing single-year MOD43B3 statistics are replaced with the associated five-year aggregate MOD43B3 statistics. This allows for a more complete description of the dormant state, while still maintaining the fidelity of the single-year data.

Pixels in tropical regions have limited and sometimes no temporal coverage due to persistent or extended seasonal cloud cover. To enhance the spatial fidelity of pixels with no temporal coverage and to provide more robust temporal trends, the five-year aggregate tropical statistics are substituted for the single-year tropical statistics. Although the unique inter-annual magnitude of each pixel's temporal trend will be maintained, the inter-annual temporal variability may be curtailed in tropical areas that rely upon these statistical instead of pixel-level trends.

Processing of year 2000 data also required special attention, as the *Terra* satellite was not operational for the first three 16-day periods (001, 017, and 033). The temporal interpolation technique, however, requires a full year's worth of data for processing. As an approximation, the five-year aggregate data and sta-

tistics were substituted directly for these three periods.

3. Trend comparison of filled and original MOD43B3 pixels

Error analysis of the spatially complete albedo products was performed in Moody et al. (2005) by comparing artificially filled values with the values actually retrieved. This paper builds upon this work by qualitatively comparing temporal and spatial trends of pixels that have been filled versus pixels flagged as original high-quality MOD43B3 data. The analysis showcases the ability of the filling technique to maintain regional and pixel-level spatial, spectral, and temporal behavior inherent in the MOD43B3 data. These comparisons will be made for both a single-year of filled data, year 2002, and for the five-year aggregate climatology product. While there will be inter-annual variations in any of the single-year products, analysis on a single year (2002) will provide an example of trends associated with the other years.

Processing Quality Assurance (QA) of the spatially complete albedo product records whether a pixel's MOD43B3 data were of high enough quality to be preserved or if they were filled using the temporal interpolation technique. Through this QA, statistics are computed for both pixels flagged as original MOD43B3 data and filled data. Trends are computed from the diffuse bihemispherical (white-sky) albedo data by ecosystem class, latitude belt, and 16-day period, as well as by global and yearly quantities.

a. Spatial and temporal variability in percentage of pixels filled

The location and percentage of pixels that are filled varies both temporally and spatially. These variations can be explored through an investigation of the percentage of pixels filled, or the number of pixels filled divided by the total number of pixels. Examining these trends can provide a sense of where there is

better temporal coverage that will thereby provide better phenological information for performing the temporal interpolation to fill missing data. While each band will have its own unique number and location of pixels filled, the variability between bands is minor. As such, data from the 0.858 μm band will be used for illustration of these trends.

To provide an overall sense of global yearly temporal coverage, Fig. 1 illustrates the number of 16-day periods that a pixel has maintained its original MOD43B3 data. Fig. 1a shows that the 2002 single-year product has limited temporal coverage in persistently cloudy regions (tropics, Southeast Asia, southern India) and the ephemeral and seasonally snow-impacted areas (Northern Hemisphere mid to high latitudes) in which the snow-free dormant state is not always observed. Some areas (in grey) have no observations at all for the entire year. Fig. 1b, the five-year aggregate climatology, shows dramatic improvements in the overall temporal coverage compared to the 2002 product. This is especially true in areas with limited or no coverage (ephemeral and seasonal snow-impacted or cloud-covered areas). This increase in temporal coverage can lead to improved description of the phenological behavior.

Global trends of where and when pixels are most likely to be filled are illustrated in Figs. 2a and 2b, respectively. Fig. 2a shows yearly statistics computed by 10° latitude belts, and confirms that snow-impacted and seasonally or persistently cloudy areas have the largest number of filled pixels, whereas mid-latitude pixels predominantly retain their original MOD43B3 data. The region with the best MOD43B3 data coverage is the 20°-40°S zone, a belt containing central and southern Australia, southern Africa, and south-central South America. This is due, with the exception of parts of South America and Africa, to this region being predominantly within the arid ecosystems of deserts and shrublands. For the

aggregate climatology, this area consists of nearly all MOD43B3 pixels, with only a fraction of a percent to a few percent containing filled pixels.

Unsurprisingly, Fig. 2b, which reveals global statistics computed for each 16-day period, demonstrates that the beginning and end of the year has the highest overall percentage of filled pixels due to the impact of ephemeral and seasonal snow. The middle of the year has the highest percentage of available MOD43B3 pixels with the tropical regions accounting for the majority of the filled pixels. For any 16-day period, the climatology has 10-20% more MOD43B3 pixels than the single-year data. On a yearly global basis, the climatology has 32% of its pixels filled compared to 47% of the single-year data.

Fig. 3 shows histograms of global yearly percentage of pixels filled by ecosystem class, highlighting which ecosystems are filled the most often. The variability is primarily due to climatology and the global distribution of ecosystem classes. It is not surprising to find that arid classes (desert, closed shrubs, permanent snow) require the least amount of filling, whereas classes predominantly in the tropics (evergreen broadleaf forest, wetlands) require the most filling of pixels. Of the forest classes, the deciduous broadleaf forest has the best coverage, primarily due to the majority of these pixels residing in the 50°-30°N and 10°-30°S latitude belts. The aggregate climatology dramatically improves the coverage of classes within the broader 50°-20°N and 10°-40°S latitude belts (deciduous broadleaf forest, cropland, crop mosaic, urban, savanna, grassland, and closed shrubs).

To provide a more in-depth analysis, statistics from three selected ecosystem classes were explored. Fig. 4 shows the percentage of pixels that were filled in for cropland, grassland, and mixed forest. These ecosystems were selected because they have distinct phenological behavior and a wide range of maximum

and minimum albedo values due to growth of the vegetation canopy. Figs. 4a-c show yearly percentages of filled pixels by 10° latitude belts, whereas Figs. 4d-f show percentage of pixels filled for 16-day trends over the latitude belt covering 50°-40°N. These analyses serve to showcase the variability in spatial and temporal MOD43B3 coverage.

The yearly trends by 10° latitude belts shown in Figs. 4a-c exhibit similar patterns for each of the three ecosystem classes. There are large amounts of filled pixels in the equatorial and high latitude zones, and conversely there are large percentages of original MOD43B3 pixels in the mid-latitudes. All exhibit local maxima in the number of filled pixels in the 30°-20°N latitude belt, primarily due to extended rain periods with persistent and seasonal clouds in India and Southeast Asia. This is especially true for cropland, which primarily resides in this region of that latitude belt. Again, the aggregate climatology consists of nearly all MOD43B3 pixels in the 20°-40°S latitude belt due to climatology and distribution of ecosystems.

Examining the temporal trends for the 50°-40°N latitude belt, shown in Figs. 4d-f, reveal that the three ecosystems exhibit trends with a high percentage of filled pixels at the beginning and end of the year due primarily to ephemeral and seasonal snow. While the single-year data exhibit inter-annual variability in ephemeral and seasonal snow effects, the averaging nature of the five-year climatology has dampened inter-annual variability. For this particular latitude belt, Grassland appears to be the least ephemeral and seasonal snow-covered ecosystem during the winter periods. Overall, the aggregate climatology is less impacted by ephemeral and seasonal snow during these times of year and once again consists almost entirely of MOD43B3 pixels in the middle of the year. Some 16-day periods have less than one percent of filled pixels during the mid-

dle of the year, especially grasslands from periods starting at days 161 to 265.

b. Spatial and temporal variability in diffuse bihemispherical (white-sky) albedo

The radiative properties of an ephemeral and seasonal snow-free surface are primarily dependent on the ecosystem classification (ground and vegetation canopy properties) and local climatology and soil condition. Spatial variability in surface properties arises both from the distribution of ecosystems, as well as the local climatology, and thereby condition of the vegetation. A pixel's radiative properties change temporally based on seasonal climatic and vegetative conditions. Vegetative surfaces exhibit defined phenological growth patterns, however inter-annual variability in climate can curtail or extend periods of productive vegetation.

These factors contribute to the spatial and temporal patterns in the diffuse bihemispherical (white-sky) albedo data shown in Fig. 5; diffuse bihemispherical albedo was selected for trend analysis as this reflectance is under conditions of isotropic illumination and thereby excludes any angular solar effects. It is important to note that the averaging nature of the five-year climatology, Figs. 5a, c, e, and g, does not allow for real interannual variability in land-cover changes. This is especially true for interannual variability during drought and extended growth seasons.

It is difficult to directly compare MOD43B3 to filled pixels or even regional trends, let alone provide a thorough error analysis, as the location of these two types of pixels are mutually exclusive. In addition, alternative (i.e. non-MODIS) validation databases suffer from the same temporal and spatial coverage issues (namely lack of observations due to cloud or ephemeral snow coverage). Nonetheless, comparing trends of latitude belt statistics can be instructive for gaining

a qualitative appreciation of how the phenological fill technique represents inherent MOD43B3 spatial and temporal variability.

Care must be taken, however, when interpreting latitude belt statistical trends as means can be skewed when contributions from regions within the latitude belt are not proportionally distributed; this scenario frequently occurs when there are relatively small numbers of either MOD43B3 or filled pixels (i.e. winter or summer, see Fig. 4). Then again, as will be explored in Sec. 3.b.1, these occurrences showcase the spatial variability inherent in the MOD43B3 product, and also the ability of the phenological fill technique to represent local behavior.

The following sub-sections will present, in a qualitative sense, a comparison of diffuse bihemispherical (white-sky) albedo temporal and spatial trends from MOD43B3 and filled latitude belt statistics. These statistics are compiled for three ecosystem classes (cropland, grassland, and mixed forest) and for three bands (0.47 μm, 0.858 μm, and the shortwave broadband 0.3-5.0 μm) to provide trends over a range of albedo values and spectral characteristics. This section will proceed by examining interlatitudinal belt variability (3.b.1) followed by an inspection of spatial (3.b.2) and temporal (3.b.3) trends.

1) INTERLATITUDINAL BELT VARIABILITY

Within a latitude belt, an ecosystem's pixels are typically distributed across several land masses, each of which has unique climatology, vegetative and ground conditions, and structure. Differences between the conditions of each region result in varying albedo magnitudes (dormant and mature) within the same ecosystem class, as seen in Fig. 5. With a (large or small) sample that is proportionately distributed across a latitude belt, these local variances are dampened and a representative latitude belt mean can be computed. However, when

the sample (large or small) is disproportionately distributed across a latitude belt, region(s) can dominate the mean calculation, resulting in a non-representative latitude belt mean.

Small samples in which a single region is wholly over- or underrepresented can exacerbate this problem. As regions (and pixels) have unique magnitudes (dormant or mature) that can vary substantially, a latitudinal mean computed from such a sample could be substantially different than if it had been computed from a proportionally distributed sample. On a positive note, these cases do provide excellent examples of the inherent MOD43B3 regional and pixel-level spatial and temporal variability. These cases also demonstrate the temporal interpolation technique's ability to maintain these inherent MOD43B3 behaviors.

Sample size also impacts the overall smoothness of the temporal trends. If, over several time periods, a sample were proportionally distributed across the latitude belt, one would expect a smooth temporal trend. Conversely, if a sample is disproportionately distributed across a latitude belt, regional values can skew the latitudinal mean; if the location of the dominant region(s) fluctuates during the time periods, the trend will appear jagged. As such, from Fig. 4 and as will be seen in the following subsections, one would expect to see the smoothest MOD43B3 trends during the middle of the year and the smoothest filled pixel trends during the beginning and end of the year.

Figure 6 illustrates this concept that disproportionately distributed contributions to the MOD43B3/fill latitudinal mean may significantly skew the calculation. This figure compares the 50°-40°N latitude belt distributions (by select 20° longitude boxes) of 2002 0.858 μm MOD43B3 and fill grassland pixels relative to the IGBP distribution for two of the least proportionally distributed time periods; Fig. 6a and 6b showcase the time periods with both the fewest number of and

least proportional distribution of MOD43B3 pixels (January 17-February 2, Julian days 17-32), and fill pixels (July 12-27, Julian days 193-208), respectively.

Fill grassland pixels (81.3%) dominate the snow-covered period shown in Fig. 6a (January 17-February 2). The remaining high-quality MOD43B3 pixels are disproportionately distributed across the latitude belt; nearly half (48.1%) of the MOD43B3 pixels (a 25.7% overrepresentation) are located between latitudes 100° to 120° E, while only 11% of the MOD43B3 pixels reside between latitudes 40° to 100°E (a 39.7% underrepresented). The overrepresented region, however, has albedo values (0.278) that are significantly higher than the remainder of the belt. The resulting MOD43B3 latitudinal mean albedo is inflated to 0.251, which is 20.12% higher than the proportionally distributed fill pixel mean (0.209). However, if both means are recalculated using the IGBP grassland distribution (i.e. precisely proportional means), the means differ by 3.3% (0.212/0.219, fill/MOD43B3).

Conversely, MOD43B3 pixels dominate (84.5%) the relatively non-obscured period shown in Fig. 6b (July 12–27). In this case, the fill pixels are disproportionately distributed; over half (54.4%) of the fill pixels (a 29.6% overrepresentation) reside between latitudes 100° to 140° E, while only 23% of the fill pixels reside between latitudes 40° to 100°E (a 27.7% underrepresented). The overrepresented region, however, has albedo values (0.338) that inflate the resulting fill latitudinal mean albedo (0.319) to be 7.6% higher than the proportionally distributed MOD43B3 mean (0.296). However, if both means are recalculated using the IGBP grassland distribution (i.e. precisely proportional means), the means differ by only 0.87% (0.301/0.298 fill/MOD43B3).

Altogether, Fig. 6 thereby highlights the inherent variability in the MOD43B3 data (Fig. 6a) as well the ability of the fill methodology to maintain the unique

phenological state of each local and regional area (Fig. 6b). Section 3.b.2 will thereby use non-proportional latitude belt means to illustrate this variability.

2) SPATIAL VARIABILITY

Figure 7 compares the spatial variability in the single-year (2002) and the aggregate climatology albedo data for a single 16-day period (Day 193, July 12-27) as a function of 10° latitude belts. For this time of year, there are few filled pixels in the 10°-40°S latitude belt; less than 10% filled pixels for single-year processing (2002) and less than 1% for the aggregate climatology. Conversely, the 0°-40°N latitude belts vary from roughly 40-90% filled pixels for the single-year processing (2002) and 20-70% filled pixels from the aggregate climatology.

For the selected ecosystems and spectral bands, the filled pixels and MOD43B3 pixels have trends that are qualitatively consistent. In the near-infrared 0.858 μm band, the cropland and mixed forest trends exhibit mature growth in the Northern Hemisphere, and are dormant in the Southern Hemisphere. The peak in the grassland occurs in the 20°-10°N latitude belt; the grassland of this region is in full growth as the Intertropical Convergence Zone (ITCZ) brings rain to this region during this time of year.

In Fig. 7, some of the MOD43B3 and filled data trends slightly diverge in the tropical latitudes. This is primarily due, as explained in Sec. 3.b.1, to the limited number of filled pixels in this region, as shown in Fig. 4. For example, in the 0°-30°S region filled grassland pixels primarily reside in South America and Northern Australia, whereas the MOD43B3 pixels are primarily from southern Africa. As the ITCZ is in northern Africa, the African grassland is senescent whereas the other continents are not. As a result, the latitudinal means of the MOD43B3 pixels are slightly lower than the filled means. These anomalies highlight the inher-

ent variability in the MOD43B3 data as well the ability of the fill methodology to maintain the unique phenological state of each local and regional area.

3) TEMPORAL VARIABILITY

The temporal variability in the single-year (2002) and aggregate climatology data can most readily be examined by focusing on a single latitude belt; the 50°-40°N latitude belt was selected as its vegetation exhibits large differences in the mean albedo values of the vegetative mature and senescent states. Fig. 8 shows latitudinal mean diffuse bihemispherical (white-sky) albedo, as a function of 16-day time period, for each of the 23 time periods and for three ecosystems.

The temporal trends show that the MOD43B3 and filled data exhibit qualitatively similar behavior, with the maximum vegetative growth and dormant states appearing qualitatively consistent (0.858 μm band best shows the vegetative trends) for both the single-year and aggregate climatology data. A closer inspection, however, reveals that there are some discrepancies. As explained in Sec. 3.b.1, these features arise from small sample sizes of MOD43B3 and filled pixels that are disproportionately distributed across the latitude belt.

For example, during the dormant stages, grasslands from the 0.858 μm 2002 single-year processed data, Fig. 4e, primarily consist of filled pixels. Examining Fig. 8d, the MOD43B3 pixels' trend in the beginning of the year differs from the filled pixels' trend, with maximum deviation occurring near the 16-day period starting at day 17 (17 Jan). During this period, only 18.7% of the latitude belt's pixels are from original MOD43B3 data. Upon closer inspection, nearly a majority (48.1%) of these MOD43B3 pixels reside in a single region located in eastern Asia. This region's dormant state has a white-sky albedo (0.278) that is higher than the spatially representative latitudinal average filled pixel state (0.209). As

such, the pixels from this area dominate the statistical computation, resulting in differing mean latitudinal MOD43B3 and filled trends during this time of year. This demonstrates the spatial and temporal variability inherent in the MOD43B3 data.

Conversely, in the aggregate climatology's grassland 0.47 μm data, Fig. 8c, the filled and MOD43B3 trends differ between days 161 and 289 (peaking at day 257). During this time, as seen in Fig. 4e, the filled pixels represent only a fraction of 1% of the total grassland pixels in this latitude belt. In fact, at the peak deviation, day 257, there are only 4,420 filled pixels, or about 0.25% of the total grassland pixels in the latitude belt. Of these 4,420 filled pixels, 4,263 pixels (96.4%) reside in a single, small region located in central Asia. This region, however, has a white-sky albedo (0.106) that differs substantially from the spatially representative MOD43B3 latitudinal average albedo (0.066). As a result, the mean filled pixel latitudinal trend deviates from the spatially representative MOD43B3 latitudinal trend during this time period. This demonstrates that the spatial and temporal uniqueness of this region is maintained by the temporal interpolation technique.

In the final analysis, the qualitatively similar MOD43B3 and fill pixel temporal trends showcase the ability of the fill technique to properly represent large scale trends; whereas the deviations in trends highlight both the inherent spatial and temporal variability in the MOD43B3 data as well the ability of the fill methodology to maintain the unique phenological state of each local and regional area.

4. Conclusions

Ephemeral and seasonal snow-free land surface albedo is an important pa-

rameter in various Earth system modeling initiatives and remote sensing and radiative transfer projects. Five years of diffuse bihemispherical (white-sky) and direct-beam directional hemispherical (black-sky) land surface albedo data have been derived from observations taken by the MODIS instrument aboard NASA's Terra satellite (MOD43B3). These data have provided researchers with a climatology of the Earth's radiative properties at fine spatial, spectral, and temporal resolutions. Missing or low-quality data, due to cloud cover and the presence of ephemeral and seasonal snow, in five years (2000-2004) of the MOD43B3 product have been filled using an updated version of an ecosystem-dependant temporal interpolation technique first reported in Moody et al. (2005).

In this paper, we describe refinements in the technique that address areas of limited observation, namely persistently cloudy (tropical) and ephemeral and seasonal snow-impacted (high latitude) regions. Also described is the creation of a spatially complete ephemeral and seasonal snow-free five-year aggregate climatology product. For this product, five years of high quality MOD43B3 observations are aggregated for each of the yearly 23 16-day time periods. The remaining missing values are filled using the refined temporal interpolation technique.

Error analysis of the interpolation technique was performed in Moody et al. (2005). This paper builds upon this work by qualitatively comparing temporal and spatial trends of data that have been filled versus data flagged as original MOD43B3 values. The analysis showcases the ability of the filling technique to maintain regional and pixel-level spatial, spectral, and temporal behavior that is inherent in the MOD43B3 data. These comparisons are made for a single-year of filled data, year 2002, and for the five-year aggregate climatology product. Single year and multi-year climatological digital data from this analysis are avail-

able for public download at ftp://modis-atmos.gsfc.nasa.gov.

Acknowledgments

The research reported in this article was supported by the MODIS Science Team under NASA contract 621-30-H4 to Goddard Space Flight Center (EGM, MDK, SP) and NASA contract NAS5-31369 to Boston University (CBS). The authors would like to express their appreciation to Dr. Lahouari Bounoua, NASA Goddard Space Flight Center, for providing valuable insight into modeling community requirements and reviewing the methodologies used in this work.

REFERENCES

Bounoua, L., R. DeFries, G. J. Collatz, P. Sellers, and H. Khan, 2002: Effects of land cover conversion on surface climate. *Climatic Change*, **52**, 29-64.

Dirmeyer, P. A. and J. Shukla, 1994: Albedo as a modulator of climate response to tropical deforestation. *J. Geophys. Res.*, **99**, 20863-20878.

Dubovik O., A. Smirnov, B. N. Holben, M. D. King, Y. J. Kaufman, T. F. Eck, and I. Slutsker, 2000: Accuracy assessments of aerosol optical properties retrieved from AERONET sun and sky-radiance measurements. *J. Geophys. Res.*, **105**, 9791-9806.

Friedl, M. A., D. K. McIver, J. C. F. Hodges, X. Y. Zhang, D. Muchoney, A. H. Strahler, C. E. Woodcock, S. Gopal, A. Schneider, A. Cooper, A. Baccini, F. Gao, and C. B. Schaaf, 2002: Global land cover mapping from MODIS: Algorithms and early results. *Remote Sens. Environ.*, **83**, 287-302.

Holben, B. N., T. F. Eck, I. Slutsker, D. Tanré, J. P. Buis, A. Setzer, E. Vermote, J. A. Reagan, Y. J. Kaufman, T. Nakajima, F. Lavenu, I. Jankowiak, and A. Smirnov, 1998: AERONET—A federated instrument network and data archive for aerosol characterization. *Remote Sens. Environ.*, **66**, 1-16.

Hsu, N. C., S. C. Tsay, M. D. King, and J. R. Herman, 2004: Aerosol retrievals over bright-reflecting source regions. *IEEE Trans. Geosci. Remote Sens.*, **42**, 557-569.

Ingram, W. J., C. A. Wilson, and J. F. B. Mitchell, 1989: Modeling climate change: An assessment of sea ice and surface albedo feedbacks. *J. Geophys. Res.*, **94**, 8609-8622.

Jin, Y., C. B. Schaaf, F. Gao, X. Li, A. H. Strahler, W. Lucht, and S. Liang, 2003a: Consistency of MODIS surface bidirectional reflectance distribution function and albedo retrievals: 1. Algorithm performance. *J. Geophys. Res.*, **108**

(D5), doi:10.1029/2002JD002803.

____, C. B. Schaaf, C. E. Woodcock, F. Gao, X. Li, A. H. Strahler, W. Lucht, and S. Liang, 2003b: Consistency of MODIS surface bidirectional reflectance distribution function and albedo retrievals: 2. Validation. *J. Geophys. Res.*, **108** (D5), doi:10.1029/2002JD002804.

Kaduk, J. and M. Heimann, 1996: A prognostic phenology scheme for global terrestrial carbon cycle models. *Climate Research*, **6**, 1-19.

Kaufman, Y. J., D. Tanré, L. A. Remer, E. F. Vermote, A. Chu, and B. N. Holben, 1997: Operational remote sensing of tropospheric aerosol over land from EOS moderate resolution imaging Spectroradiometer. *J. Geophys. Res.*, **102**, 17051-17067.

King, M. D. and D. D. Herring, 2000: Monitoring Earth's vital signs. *Sci. Amer.*, **282**, 72-77.

____, Y. J. Kaufman, W. P. Menzel, and D. Tanré, 1992: Remote sensing of cloud, aerosol, and water vapor properties from the Moderate Resolution Imaging Spectrometer (MODIS). *IEEE Trans. Geosci. Remote Sens.*, **30**, 2-27.

____, Y. J. Kaufman, D. Tanré, and T. Nakajima, 1999: Remote sensing of tropospheric aerosols from space: Past, present, and future. *Bull. Amer. Meteor. Soc.*, **80**, 2229-2259.

____, W. P. Menzel, Y. J. Kaufman, D. Tanré, B. C. Gao, S. Platnick, S. A. Ackerman, L. A. Remer, R. Pincus, and P. A. Hubanks, 2003: Cloud and aerosol properties, precipitable water, and profiles of temperature and humidity from MODIS. *IEEE Trans. Geosci. Remote Sens.*, **41**, 442-458.

____, S. Platnick, P. Yang, G. T. Arnold, M. A. Gray, J. C. Riédi, S. A. Ackerman, and K. N. Liou, 2004: Remote sensing of liquid water and ice cloud optical thickness and effective radius in the arctic: Application of airborne multis-

pectral MAS data. *J. Atmos. Oceanic Technol.*, **21**, 857-875.

Liang, S. L., H. L. Fang, M. Z. Chen, C. J. Shuey, C. Walthall, C. Daughtry, J. Morisette, C. Schaaf, and A. Strahler, 2002: Validating MODIS land surface reflectance and albedo products: Methods and preliminary results. *Remote Sens. Environ.*, **83**, 149-162.

Moody, E. G., M. D. King, S., Platnick, C. B. Schaaf, and F. Gao, 2005: Spatially complete global spectral surface albedos: Value-added datasets derived from Terra MODIS land products. *IEEE Trans. Geosci. Remote Sens.*, **43**, 144–158.

Penuelas, J., I. Filella, X. Zhang, L. Llorens, R. Ogaya, F. Lloret, P. Comas, M. Estiarte, and J. Terradas, 2004: Complex spatiotemporal phenological shifts as a response to rainfall changes. *New Phytologist*, **161**, 837-846.

Platnick, S., M. D. King, S. A. Ackerman, W. P. Menzel, B. A. Baum, J. C. Riédi, and R. A. Frey, 2003: The MODIS cloud products: Algorithms and examples from Terra. *IEEE Trans. Geosci. Remote Sens.*, **41**, 459-473.

Reed, B. C., J. F. Brown, D. VanderZee, T. R. Loveland, J. W. Merchant, and D. O. Ohlen, 1994: Measuring phenological variability from satellite imagery. *J. Veg. Sci.*, **5**, 703-714.

Schaaf, C. B., F. Gao, A. H. Strahler, W. Lucht, X. W. Li , T. Tsang, N. C. Strugnell, X. Y. Zhang, Y. F. Jin, J. P. Muller, P. Lewis, M. Barnsley, P. Hobson, M. Disney, G. Roberts, M. Dunderdale, C. Doll, R. P. d'Entremont, B. X. Hu, S. L. Liang, J. L. Privette, and D. Roy, 2002: First operational BRDF, albedo nadir reflectance products from MODIS. *Remote Sens. Environ.*, **83**, 135-148.

Schwartz, M. D., 1998: Green-wave phenology. *Nature*, **394**, 839-840.

____ and B. C. Reed, 1999: Surface phenology and satellite sensor-derived onset of greenness: An initial comparison. *Int. J. Remote Sens.*, **20**, 3451-3457.

Sellers, P. J., D. A. Randall, G. J. Collatz, J. A. Berry, C. B. Field, D. A. Dazlich, C. Zhang, and L. Bounoua, 1996: A revised land surface parameterization (SiB2) for atmospheric GCMs. Part 1: Model formulation. *J. Climate*, **9**, 676-705.

Wang, K., J. Liu, X. Zhou, M. Sparrow, M. Ma, Z. Sun, and W. Jiang, 2004: Validation of the MODIS global albedo surface albedo product using ground measurements in a semidesert region on the Tibetan Plateau. *J. Geophys. Res.*, **109** (D5), doi:10.1029/2003JD004229.

White, M. A., P. E. Thornton, and S. W. Running, 1997: A continental phenology model for monitoring vegetation responses to interannual climatic variability. *Global Biogeochem. Cycles*, **11**, 217-234.

Whitlock, C. H., T. P. Charlock, W. F. Staylor, R. T. Pinker, I. Laszlo, A. Ohmura, H. Gilgen, T. Konzelman, R. C. DiPasquale, C. D. Moats, S. R. LeCroy, and N. A. Ritchey, 1995: First global WCRP shortwave surface radiation budget data set. *Bull. Amer. Meteor. Soc.*, **76**, 905-922.

Zhang, S., M. A. Friedl, C. B. Schaaf, A. H. Strahler, J. C. F. Hodges, F. Gao, and B. C. Reed, 2003: Monitoring vegetation phenology using MODIS. *Remote Sens. Environ.*, **84**, 471-475.

FIGURE LEGENDS

Fig. 1. Number of high quality MOD43B3 retrievals preserved for each pixel in the spatially complete (a) single-year 2002 and (b) five-year (2000-2004) aggregate climatology albedo data. As each year of data is comprised of 23 16-day periods, the maximum, shown in red, is 23; zero observations appear as grey. Mid-latitude regions typically have more observations than areas of persistent clouds (tropics) or ephemeral and seasonal snow and low illumination angles (high latitudes). The aggregate product generally provides more complete temporal information than any single year of data.

Fig. 2. Percentage of pixels filled in, given as trends of (a) yearly percentage by 10° latitude belts, and (b) global percentage by day of year. The trends are calculated from the 0.858 μm band for the five-year aggregate climatology and 2002 single-year albedo data.

Fig. 3. Histogram of global yearly percentage of pixels filled in, given by ecosystem class. The statistics are computed from the 0.858 μm band for the five-year aggregate climatology and 2002 single-year albedo data.

Fig. 4. Percentage of pixels filled in, given as trends of (a)-(c) yearly percentage by 10° latitude belts, and (d)-(f) percentage by day of year over the 50°-40°N latitude belt. The trends are computed for three ecosystem classes, cropland (a and d), grassland (b and e), and mixed forest (c and f). The statistics are calculated from the 0.858 μm band for the five-year aggregate climatology and 2002 single-year albedo data.

Fig. 5. Spatially complete diffuse bihemispherical (white-sky) albedo at 0.86 μm for the 16-day periods of (a, b) January 1-16, (c, d) April 3-18, (e, f) July 12-27, and (g, h) September 30-October 14. Data from the five-year

(2000-2004) climatology is presented in the left column (a, c, e, g), while the single-year 2002 albedo data is presented in the right column (b, d, f, h). To emphasize variability in albedo due to vegetation, areas of high reflectivity (above 0.5) are shown in grey.

Fig. 6. Distribution (as a percentage) of 50°-40°N (by select 20° longitude boxes) 2002 0.858 μm fill and MOD43B3 diffuse bihemispherical (white-sky) albedo grassland pixels relative to the IGBP baseline distribution. Fig. 6a and 6b represent the relative distributions during the January 17-February 2 (Julian days 17-32) and July 12-27 (Julian days 193-208) 16-day periods, respectively.

Fig. 7. Mean diffuse bihemispherical (white-sky) albedo values computed by 10° latitude belts for three bands (0.47 and 0.858 μm narrowband, and the 0.3-5.0 μm shortwave broadband) during the 16-day period of July 12-27 (data day 193). Trends are computed for three ecosystem classes, cropland (a and b), grassland (c and d), and mixed forest (e and f) from the five-year aggregate climatology (a, c, and e) and the 2002 single-year albedo data (b, d, and f).

Fig. 8. Mean diffuse bihemispherical (white-sky) albedo values computed for each 16-day period for three bands (0.47 and 0.858 μm narrowband, and the 0.3-5.0 μm shortwave broadband) over the 50°-40°N latitude belt. Trends are computed for three ecosystem classes, cropland (a and b), grassland (c and d), and mixed forest (e and f) from the five-year aggregate climatology (a, c, and e) and the 2002 single-year albedo data (b, d, and f).

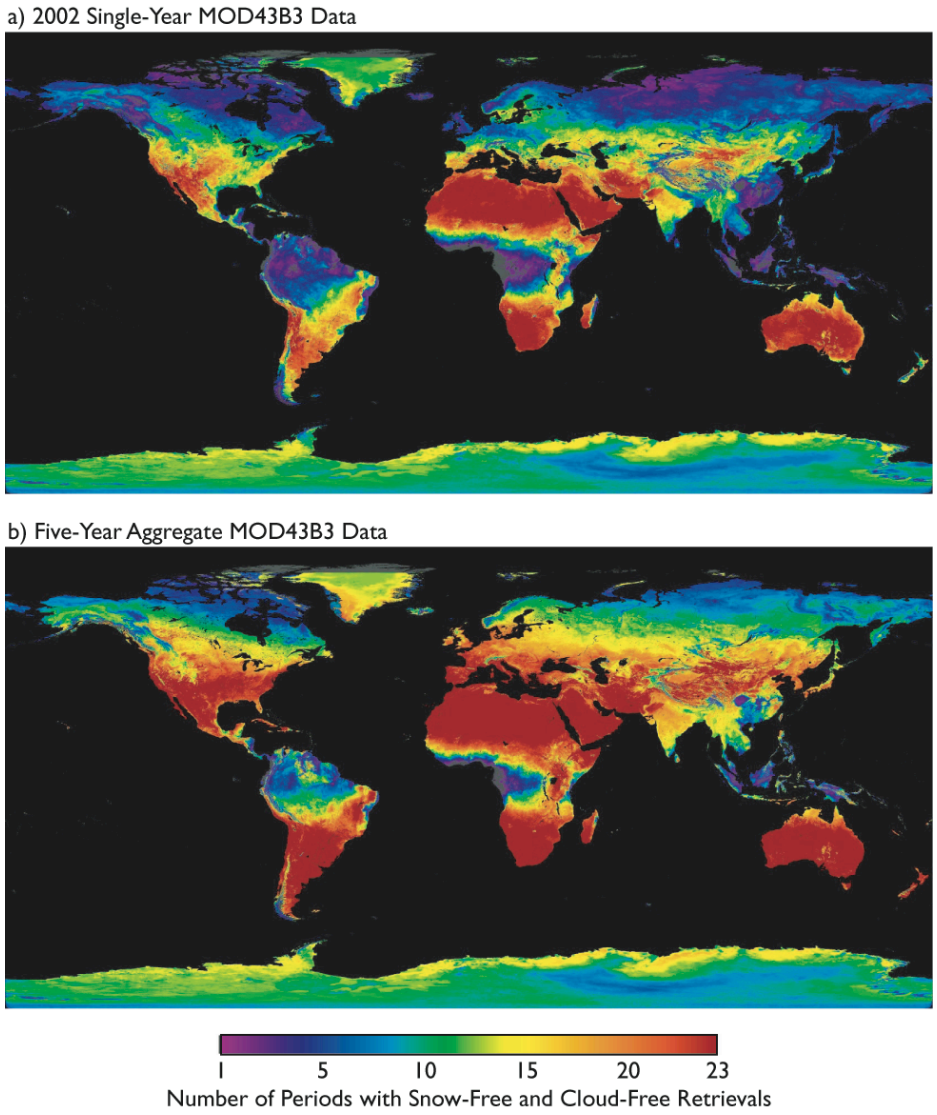

Fig. 1. Number of high quality MOD43B3 retrievals preserved for each pixel in the spatially complete (a) single-year 2002 and (b) five-year (2000-2004) aggregate climatology albedo data. As each year of data is comprised of 23 16-day periods, the maximum, shown in red, is 23; zero observations appear as grey. Mid-latitude regions typically have more observations than areas of persistent clouds (tropics) or ephemeral and seasonal snow and low illumination angles (high latitudes). The aggregate product generally provides more complete temporal information than any single year of data.

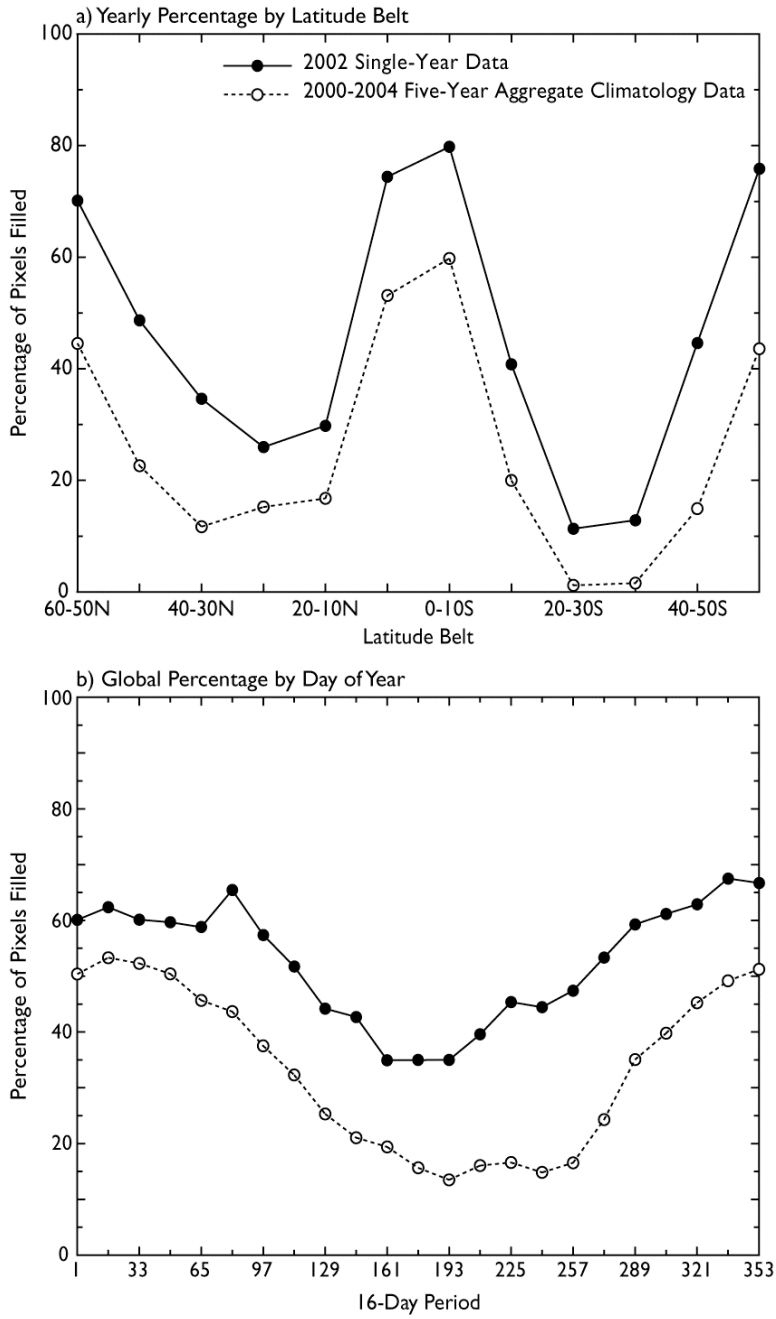

Fig. 2. Percentage of pixels filled in, given as trends of (a) yearly percentage by 10° latitude belts, and (b) global percentage by day of year. The trends are calculated from the 0.858 μm band for the five-year aggregate climatology and 2002 single-year albedo data.

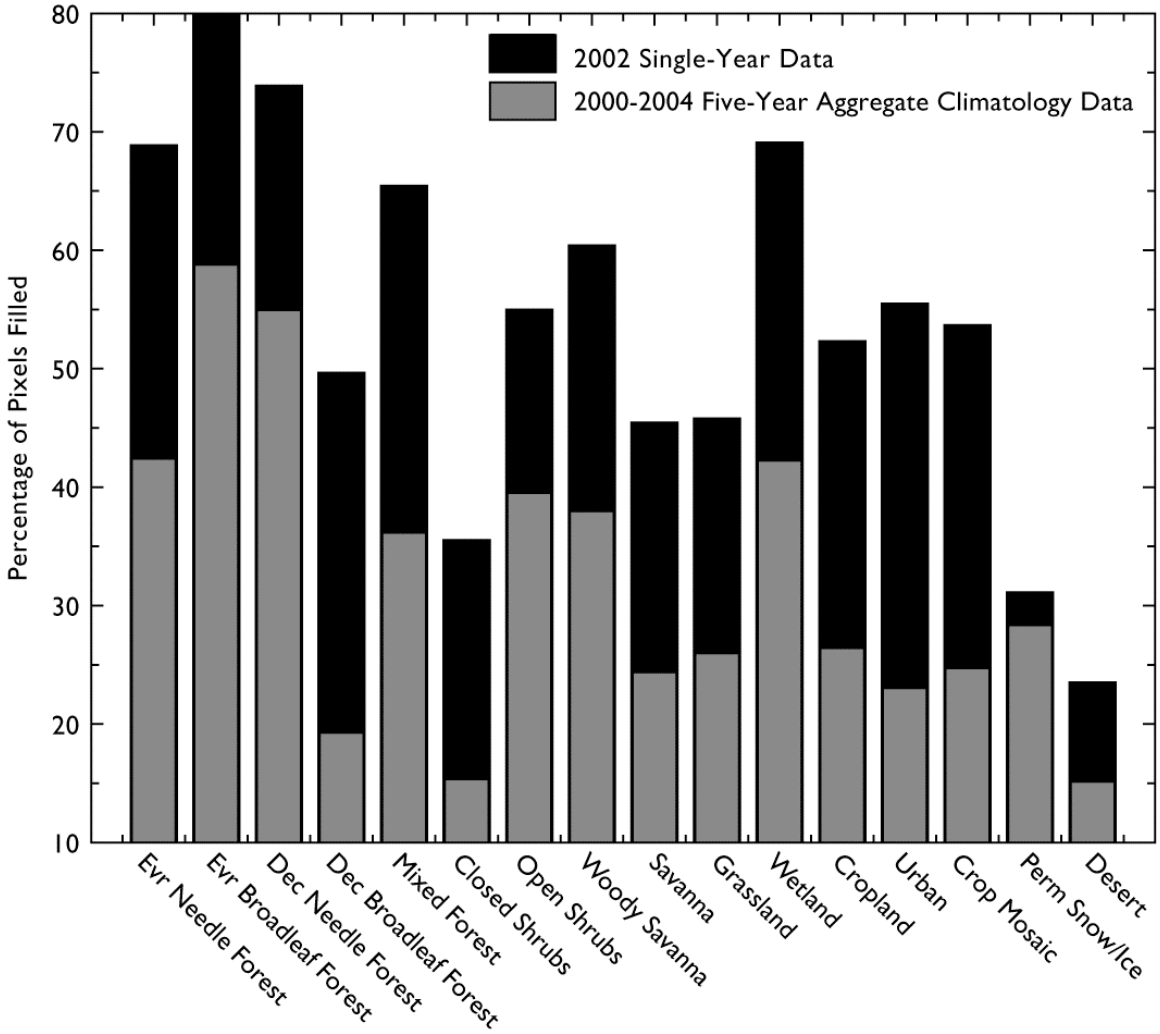

Fig. 3. Histogram of global yearly percentage of pixels filled in, given by ecosystem class. The statistics are computed from the 0.858 μm band for the five-year aggregate climatology and 2002 single-year albedo data.

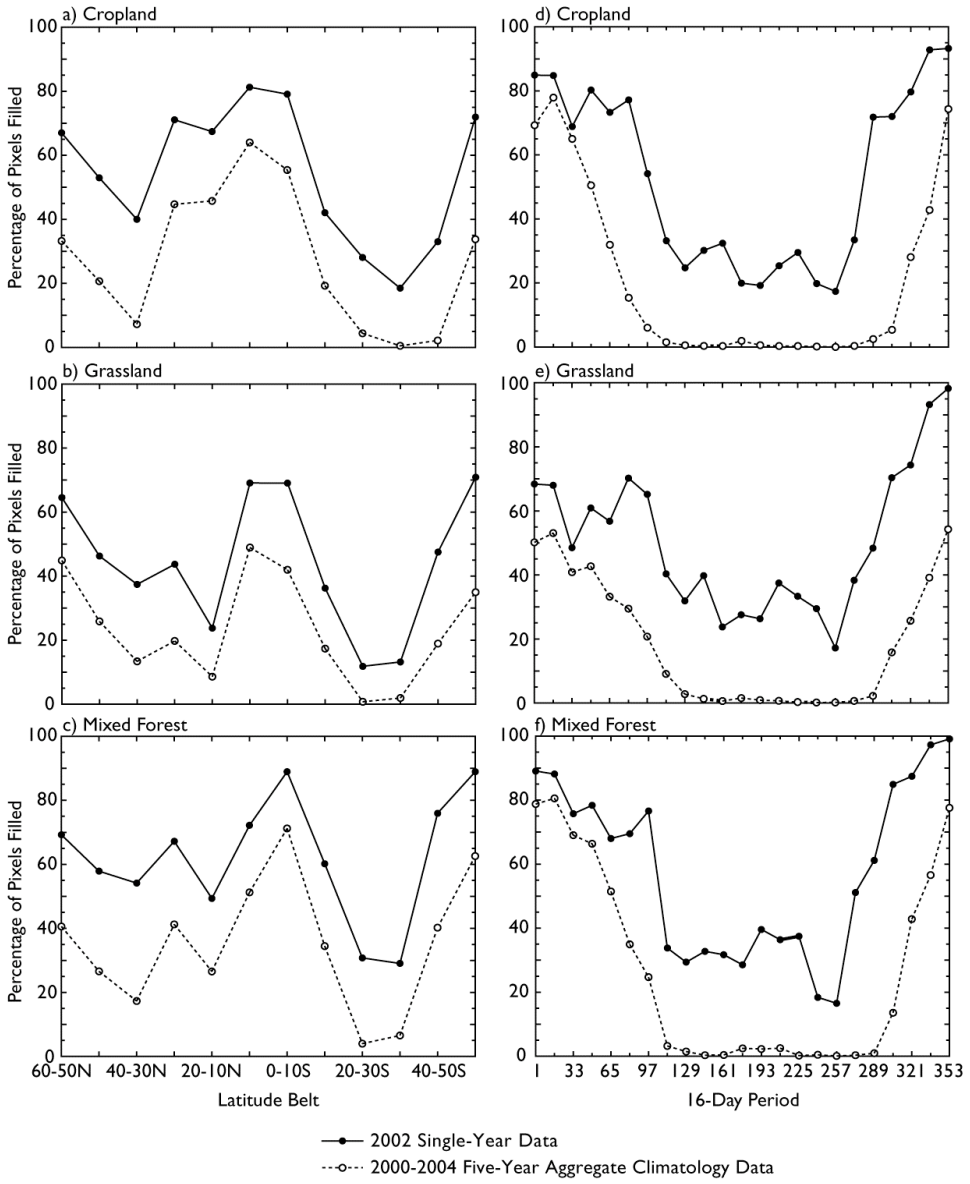

Fig. 4. Percentage of pixels filled in, given as trends of (a)-(c) yearly percentage by 10° latitude belts, and (d)-(f) percentage by day of year over the 50°-40°N latitude belt. The trends are computed for three ecosystem classes, cropland (a and d), grassland (b and e), and mixed forest (c and f). The statistics are calculated from the 0.858 μm band for the five-year aggregate climatology and 2002 single-year albedo data.

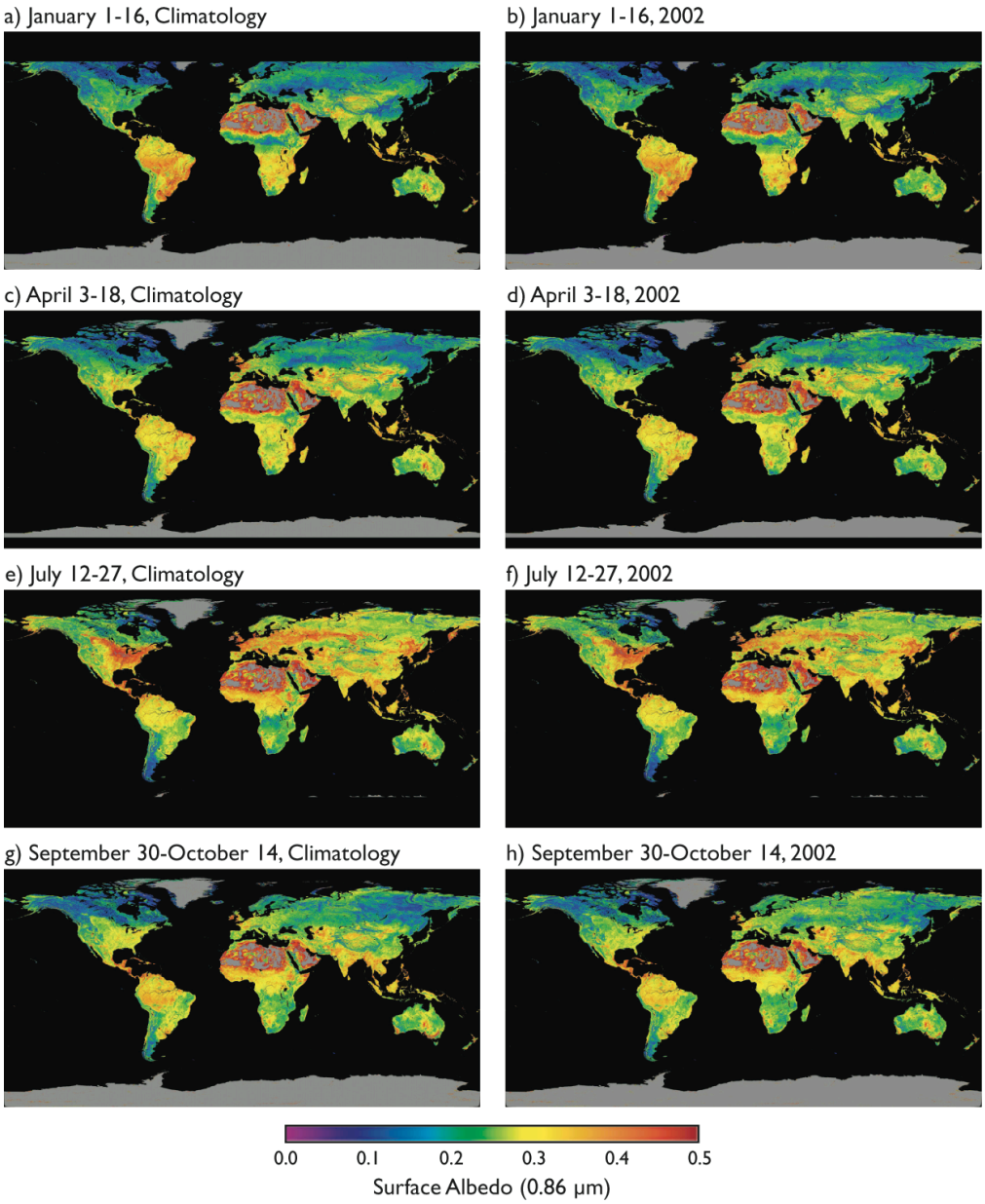

Fig. 5. Spatially complete diffuse bihemispherical (white-sky) albedo at 0.86 μm for the 16-day periods of (a, b) January 1-16, (c, d) April 3-18, (e, f) July 12-27, and (g, h) September 30-October 14. Data from the five-year (2000-2004) climatology is presented in the left column (a, c, e, g), while the single-year 2002 albedo data is presented in the right column (b, d, f, h). To emphasize variability in albedo due to vegetation, areas of high reflectivity (above 0.5) are shown in grey.

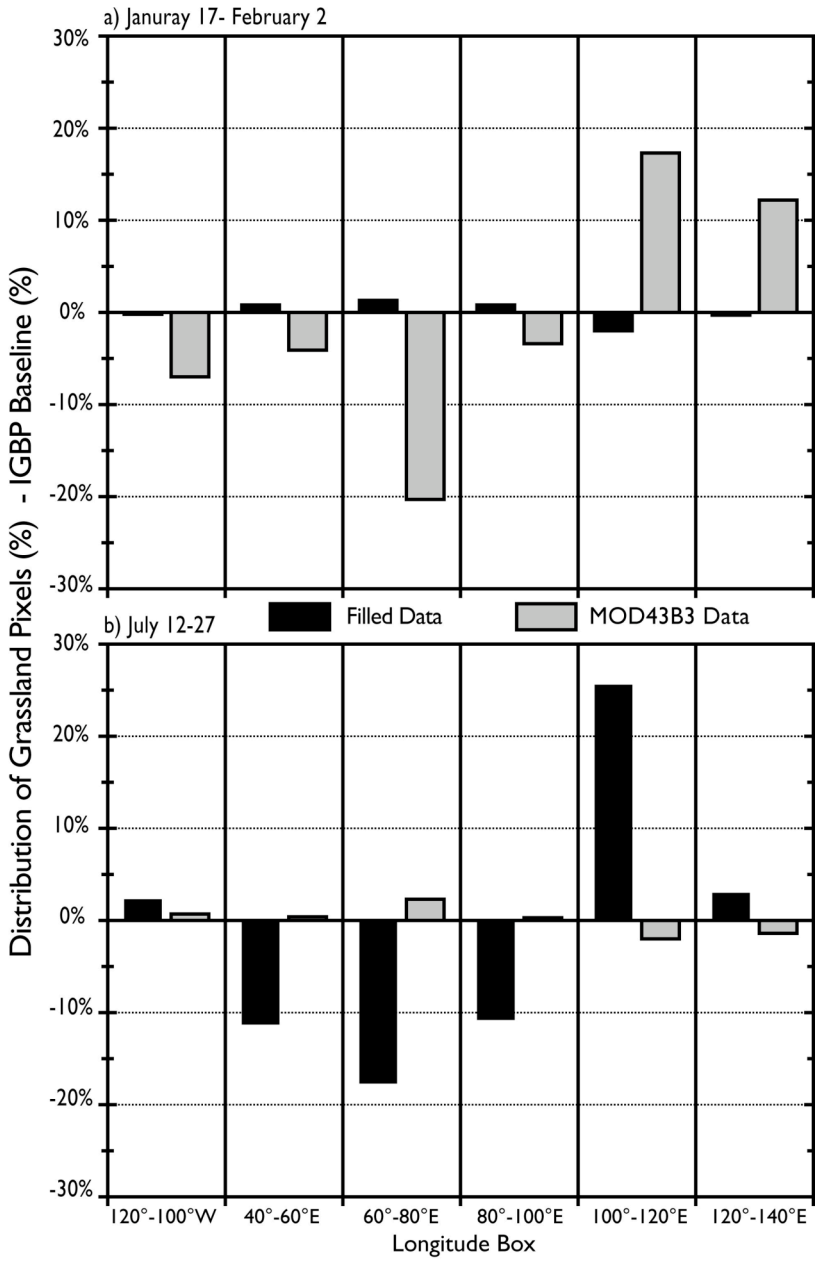

Fig. 6. Distribution (as a percentage) of 50°-40°N (by select 20° longitude boxes) 2002 0.858 μm fill and MOD43B3 diffuse bihemispherical (white-sky) albedo grassland pixels relative to the IGBP baseline distribution. Fig. 6a and 6b represent the relative distributions during the January 17-February 2 (Julian days 17-32) and July 12-27 (Julian days 193-208) 16-day periods, respectively.

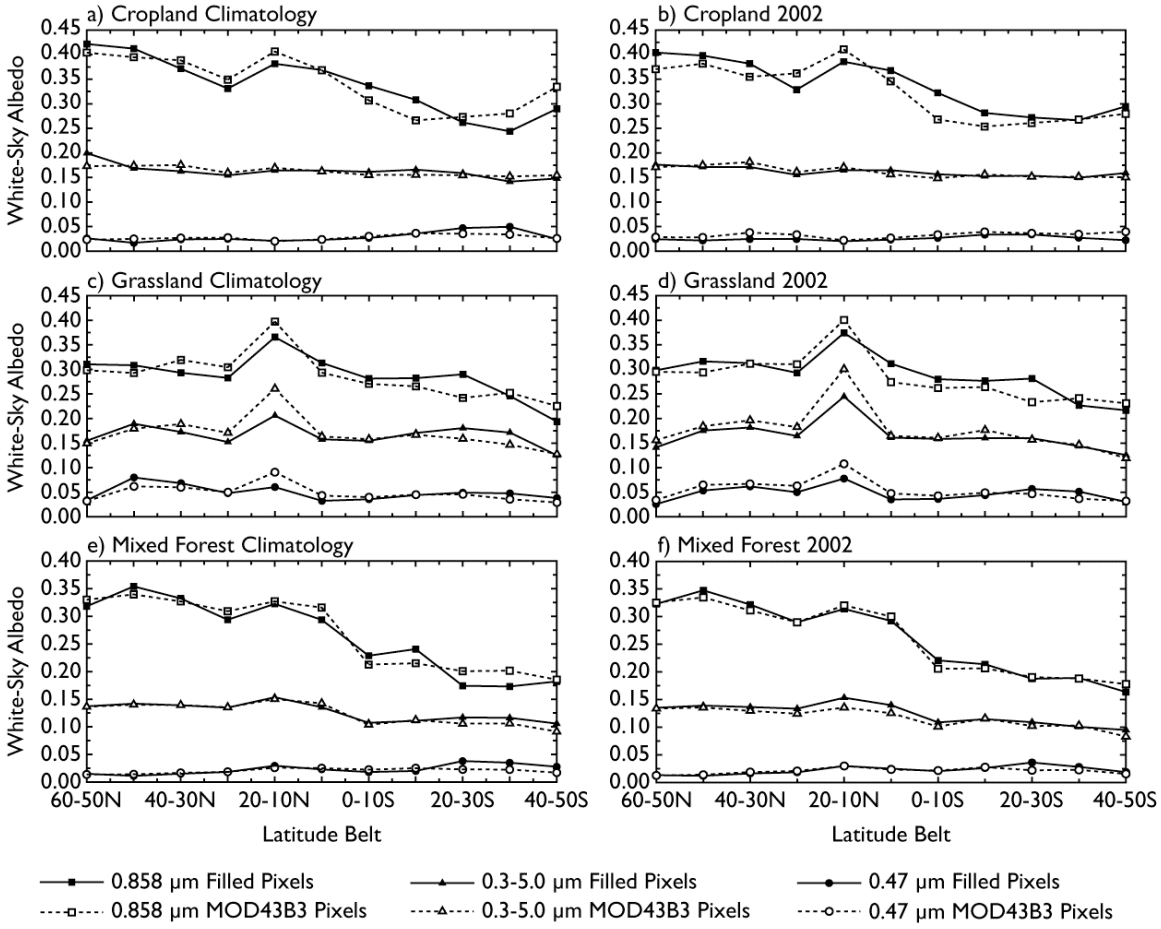

Fig. 7. Mean diffuse bihemispherical (white-sky) albedo values computed by 10° latitude belts for three bands (0.47 and 0.858 μm narrowband, and the 0.3-5.0 μm shortwave broadband) during the 16-day period of July 12-27 (data day 193). Trends are computed for three ecosystem classes, cropland (a and b), grassland (c and d), and mixed forest (e and f) from the five-year aggregate climatology (a, c, and e) and the 2002 single-year albedo data (b, d, and f).

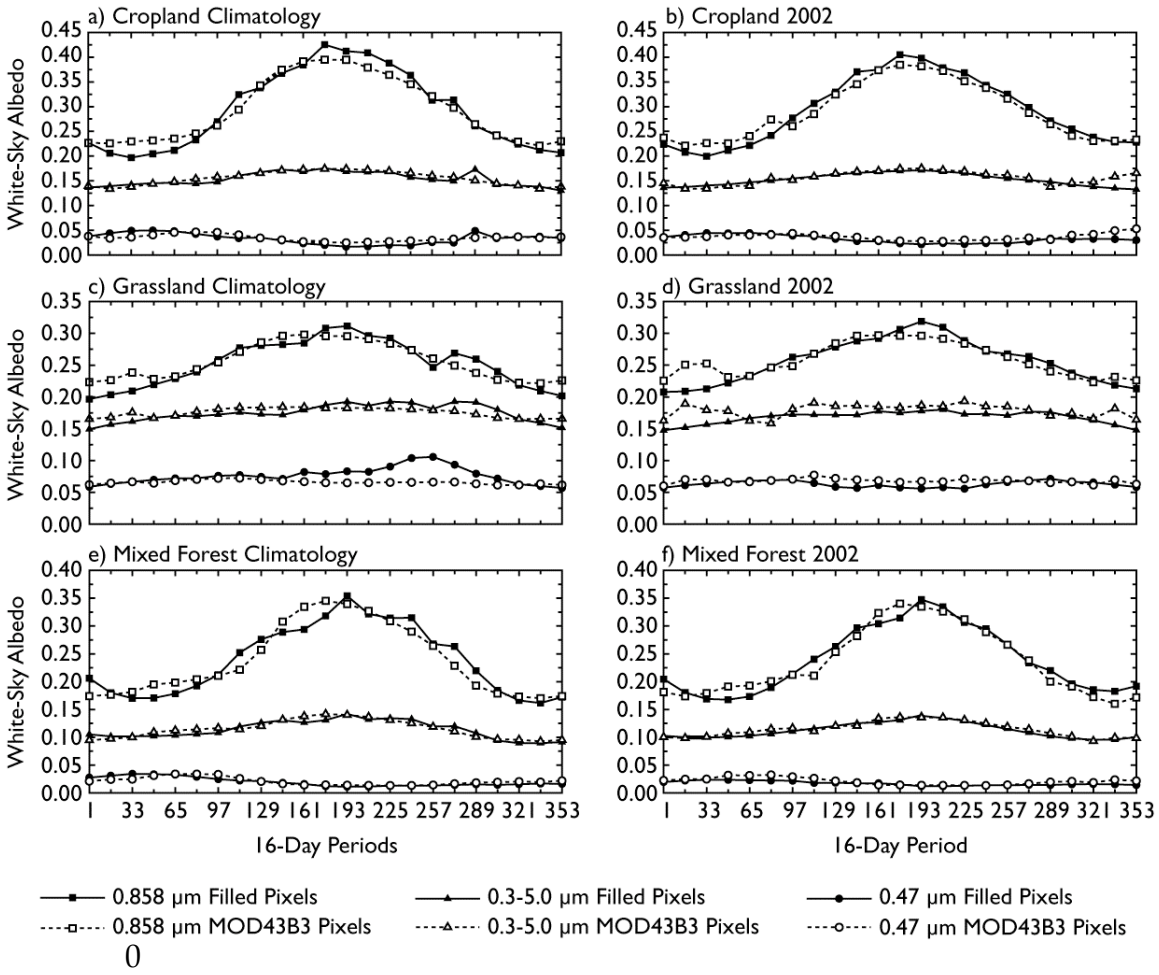

0

Fig. 8. Mean diffuse bihemispherical (white-sky) albedo values computed for each 16-day period for three bands (0.47 and 0.858 μm narrowband, and the 0.3-5.0 μm shortwave broadband) over the 50°-40°N latitude belt. Trends are computed for three ecosystem classes, cropland (a and b), grassland (c and d), and mixed forest (e and f) from the five-year aggregate climatology (a, c, and e) and the 2002 single-year albedo data (b, d, and f).